Properties of microinjection molding of polymer multiwalled carbon nanotube conducting composites

Abbasi, Samaneh; Derdouri, Abdessalem; Carreau, Pierre J.

Publisher's version / Version de l'éditeur:
https://doi.org/10.1002/pen.21904
Polymer Engineering and Science, 51, 5, pp. 992-1003, 2011-03-07

Properties of Microinjection Molding of Polymer Multiwalled Carbon Nanotube Conducting Composites

Samaneh Abbasi,[1] Abdessalem Derdouri,[2] Pierre J. Carreau[1]
[1] *CREPEC, Department of Chemical Engineering, Ecole Polytechnique, Montreal, QC, Canada*

[2] *CREPEC, Industrial Materials Institute, National Research Council Canada, Boucherville, QC, Canada*

The effects of processing conditions on the microstructure and properties of polypropylene/multiwalled carbon nanotube (PP/MWCNT) and polycarbonate/multiwalled carbon nanotube (PC/MWCNT) composites were studied. Samples of various MWCNT loadings were prepared by diluting commercial masterbatches. Different processing conditions were then used to systematically change the degree of nanotube alignment, from random to highly aligned. The crystallinity of the PP/MWCNT nanocomposites was found to go through a maximum as a function of nanotube content while the overall rate of crystallization increased. For the highly sheared microinjected PP/MWCNT samples well oriented crystals were formed. Electrical conductivity of the nanocomposites was improved by the presence of the crystalline structure; however, the high degree of nanotube alignment in the microparts resulted in a significant increase in the electrical percolation threshold. The PP nanocomposites exhibited mechanical properties significantly enhanced by nanotube loading; this effect was small in the case of the PC nanocomposites. POLYM. ENG. SCI., 51:992–1003, 2011. © 2011 Society of Plastics Engineers

INTRODUCTION

After their discovery in 1991 by Iijima [1, 2] carbon nanotubes (CNTs) became attractive candidates for fundamental investigations due to their unique electronic structure and extraordinary properties. Since then, an extensive research effort has been devoted to the nanotube fabrication, characterization, and development of applications [3]. Their intrinsic structure, size scale and aspect ratio suggest a variety of applications such as nanoelectronics, sensors, and field emission as well as high performance nanocomposites.

Correspondence to: Pierre J. Carreau; e-mail: pcarreau@polymtl.ca
Contract grant sponsor: NSERC (Natural Science and Engineering Research Council of Canada).
DOI 10.1002/pen.21904
Published online in Wiley Online Library (wileyonlinelibrary.com).

Recently, considerable attention has been devoted to carbon nanotube/polymer composites from both processing and application points of view. Besides the individual properties of carbon nanotubes, numerous potential benefits are expected when they are employed as reinforcing agents in nanocomposites. One of the key interest in carbon nanotubes incorporated into polymeric materials stems from their potential to develop conductive polymer composites at relatively low concentrations [4–9].

The high electrical conductivity in conductive particles based nanocomposites is explained in term of percolation i.e., the structure in which the particles touch one another, resulting in a continuous electrically conductive path. The filler concentration at which the electrical conductivity increases abruptly is known as the percolation threshold. It depends not only on the types of filler and polymer but also on the dispersion state of the filler and the morphology of the matrix [10–13].

The percolation threshold is found to be much higher in the case of thermoplastic matrices [8, 14-17] in comparison to thermoset filled systems [18]. In semicrystalline matrices, additional complexity arises due to the crystallization induced phase separation and subsequent rejection of the nanotubes by the advancing crystalline phase [19, 20]. It is well known that carbon nanotubes are well dispersed in polar polymers such as poly (methyl-methacrylate) (PMMA) [15] and polycarbonate (PC) [16]. However, in nonpolar polymers such as polypropylene (PP), CNT dispersion remains a big challenge and might affect the percolation threshold as well.

Incorporation of carbon particles into incompatible polymer blends can provide them with electrical conductivity at very low filler content due to a double percolation phenomenon [21, 22]. Double percolation refers to the structure in which there are two types of percolation in the same composite material. The first one, which is typically observed in reinforced composite materials, is associated with the electrical continuity of the conductive particles in the filler-rich phase and the second one is associated with the continuity of this phase in the blend. The improvement in electrical conductivity will depend on the conductive

particle concentration threshold in the filler-rich phase and on the volume fraction of the filler-rich phase required to induce co-continuity in the blend [22].

It is well known that the microstructure of plastic parts is the result of complex changes imposed to the base polymer by special processing conditions [23]. Typical thermoplastic processing involves pellets melting, plastication, melt flow, pressurization and shaping and finally solidification from the molten state, either by crystallization or vitrification. The complex thermo-mechanical history imposed on the polymer during processing leads to substantial spatial variations of chain orientation under shear and elongational flows and to the formation of a superstructure controlled by the local dynamics of the process. These effects result in a large anisotropy of the final physical properties particularly if the polymer is semicrystalline and is filled with particles of large aspect ratio (glass or carbon fibers, clay or mica platelets, carbon nanotubes, or nanofibrils, etc.). The objective of this work is to develop a clear understanding of how processing conditions influence the nanotube network and subsequently the nanocomposites properties.

With the recent trend towards product miniaturization, the rapid development of microsystem technologies has opened up new applications for polymer nanocomposites. Particularly, carbon nanotube based polymer composites are suitable candidates for the fabrication of microscale components where the nano size of the added particles is an advantage and only grams of materials are necessary to manufacture high-valued products. A number of processing technologies have been explored to produce polymer-based microdevices amongst which microinjection molding is one of the most suitable for producing microparts cheaply and with high precision. Microinjection molded parts are defined as (1) parts with a weight grams down to milligrams, (2) parts with microstructured regions, and (3) parts with microprecision dimensions. In the first category the parts have masses of a few milligrams, but their dimensions are not necessarily on the micron scale. Parts of the second category are characterized by local micro features on the micron order, such as microholes and slots. The third category includes parts of any dimensions that have tolerances in the micron range [24].

As in the case of conventional injection molding, the properties of parts made by microinjection molding are strongly affected by the processing parameters. However, because of the exceptional characteristics of microinjection molding, these parameters and their effects are not necessarily the same as encountered in conventional molding. Microinjection molding features extreme injection pressures, very high shear and cooling rates as well as very short cycle times compared to the conventional process. Significant reports on microinjection molding appeared during this decade most of which were on neat polymers [25–29]. Some studies did consider polymer compounds containing fillers such as short glass fibers, glass particles, and nanoceramic materials as illustrated by the work of Huang et al. [30, 31].

Another interesting processing alternative for producing microparts is microinjection-compression molding. This process is regarded as an extension of microinjection molding by incorporating a compression phase to compact the material inside the mold cavity. After injection of the melt into a slightly open mold, the polymer proceeds to the extremities of the cavity under relatively low pressure and stress [32] as the mold closes fully.

It is the aim of this study to investigate the influence of crystalline structure, nanotube loading and microinjection molding conditions on the properties of polymer/MWCNT nanocomposites with a special focus on the electrical conductivity. To this end, we chose two polymers, a polar amorphous polycarbonate (PC) and an isotactic polypropylene (iPP) as a nonpolar semicrystalline polymer. Polycarbonate, a typical amorphous polymer, is an important commercially available engineering thermoplastic for injection molding applications because of its excellent processability and mechanical properties. Recently, carbon nanotubes have been used as a special filler to be incorporated into PC for stiffness reinforcement as well as thermal and electrical conductivity enhancement [8, 14, 33–36]. Polypropylene is also one of the most commonly used polymers in the preparation of such nanocomposites owing to its well-balanced physical and mechanical properties combined with benefits like low cost, low density, good processability, and wide range of applications [37–40]. However, PP exhibits very poor compatibility and low adhesion to other polymers and inorganic fillers due to its nonpolarity and crystallizability. It has been found that in PP/clay nanocomposites crystallization of the PP matrix led to the expulsion of clay platelets from the crystalline phase by thermodynamic forces [41]. A similar phenomenon is expected to occur when carbon nanotubes are used instead of clay platelets. Their rejection by the growing crystalline phase may result in a conductive nanotubes network at lower concentrations according to the concept of double percolation.

We optimized the nanocomposites preparation to obtain the best possible nanotube dispersion as observed by transmission electron microscopy (TEM) and scanning electron microscopy (SEM). Thereafter, samples were prepared by compression molding and micromolding under different processing conditions and using different cavity shapes. Finally, we employed a variety of characterization methods to investigate the effect of the processing conditions on the structure and properties of the polymer/CNTs composites.

EXPERIMENTAL

Materials

Masterbatches of 20 wt% MWCNT in PP and 15 wt% MWCNT in PC were purchased from Hyperion Catalysis

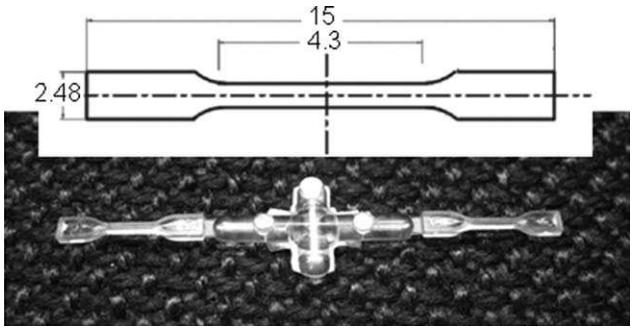

FIG. 1. Microinjected tensile bar produced using a mold with dog-bone shape cavity (dimensions in the sketch are in mm).

International, Cambridge, MA. According to the supplier, the carbon nanotubes are vapor grown and typically consist of 8–15 graphite layers wrapped around a hollow 5-nm core [42]. The diameter range was stated to vary from 15 to 50 nm and the length range between 1 and 10 μm as confirmed by TEM characterization. The masterbatches were then diluted with a polycarbonate (Calibre 1080) supplied by DOW Chemical and with an isotactic polypropylene (PP HD120) supplied by Borealis Co. to prepare nanocomposite samples of various loadings. The polycarbonate (PC1080) has a density of 1200 kg/m^3 according to ASTM D792, with a melt flow rate of 11 g/10 min at 250°C and a water absorption of 0.20% after 24 h at 23°C according to ASTM D570. The polypropylene (PP HD120) has a density of 908 kg/m^3 according to ASTM D792, with a melt flow rate of 8 g/10 min at 230°C. A polypropylene grafted maleic anhydride (PP-g-MA Polybond PB3150 with 0.5 wt% MA and with a melt flow rate of 20 g/10 min at 190°C) was used as a compatibilizer in an attempt to improve the nanotube dispersion in PP/MWCNT nanocomposites.

Nanocomposite Preparation and Molding

The composites were made by melt mixing the masterbatches with the neat polymers. The polycarbonate and PC/MWCNT masterbatch were dried for a minimum of 4 h at 120°C prior to mixing. The polypropylene, PP/MWCNT and PP-g-MA were also dried for 1 h at 90°C. Six samples with MWCNT contents between 0.5 and 15 wt% were prepared using a lab twin-screw extruder, Leistritz ZSE 18HP, operating at 100 rpm and 210°C for the PC and at 250 rpm and 190°C for the PP nanocomposites (conditions previously optimized via a set of controlled experiments). Microinjection molding and microinjection-compression molding were then employed to produce parts of different shapes and dimensions. Prior to each process, the nanocomposites were dried under the conditions previously mentioned. Compression molded disks were also prepared (Carver laboratory press, model 3912) to compare the nanocomposite properties before and after microinjection molding. Microinjection molding was done using a Battenfeld Microsystem 50 machine. In the case of the PC/MWCNT nanocomposites, injection was done at an average barrel temperature of 300°C and under a pressure of ~100 MPa while the injection speed was constant at 400 mm/s. The mold temperature was kept constant at 80°C and the cooling time was set to 10 s. For the PP/MWCNT nanocomposites, we used an average barrel temperature of 260°C, a pressure of ~100 MPa and a constant injection speed of 400 mm/s. To reduce shrinkage the mold temperature was optimized and kept constant at 20°C while the cooling time was set to 10 s. For mechanical tests, we used a mold with the dog-bone shape cavity of 15 mm long, with the center section of 1 mm wide by 0.78 mm thick by 4.3 mm long, gated at one end (see Fig. 1); while the electrical measurements were done using a disk shape mold of 25 mm in diameter and 1 mm thick, gated at the centre. Finally, microinjection-compression molding was employed to evaluate the effect of applying a compression step at the end of the injection phase on the part properties, using the centrally gated disk cavity with the same dimensions as described before. The process consisted of injecting the melt into the cavity, while the mold was not totally closed. This led to an initial cavity filling under a lower pressure than if the mold was closed. After the injection stage, the mold was closed to compress the melt and to completely fill the cavity. The operating conditions in this experiment were the same as for microinjection molding in the injection phase, while during the compression phase, the mold closing speed and gap used were set to 1.5 mm/s and 1.2 mm, respectively.

Morphological Characterization

The morphology of the nanocomposites was studied through scanning and transmission electron microscopy (SEM, TEM). For SEM we used a high resolution Hitachi S-4700 microscope. In the case of PC nanocomposite, SEM was done on the surface of an ultramicrotomed sample cut with a diamond knife at room temperature. The surface of the PP nanocomposite sample was etched using a potassium permanganate solution to eliminate the amorphous phase from the surface. The quality of the dispersion could be seen much better with this method rather than using an ultramicrotomed surface. All SEM samples were then coated with a vapor deposit of platinum for 25 s. TEM was done on ultrathin nanocomposites cross-sections for a better observation of the morphology, using a Hitachi HD-2000 microscope.

Crystallinity Measurements

Differential scanning calorimetry (DSC) and X-ray diffraction (XRD) were used to study the crystallization behavior of PP/MWCNT nanocomposite. Nonisothermal crystallization analysis was performed using a TA instrument Q-100 differential scanning calorimeter. Samples of about 5–10 mg were heated from 25 to 260°C at a heating

 DOI 10.1002/pen

rate of 10°C/min and then held for 5 min to eliminate the thermal history of the materials. The samples were subsequently cooled to 25°C at a cooling rate of 10°C/min before starting a second heating at the same rate to the same final temperature. The degree of crystallinity was calculated using the following equation [43]:

$$X_c = \frac{\Delta H_f}{\Delta H_f^0 (1 - w)} \times 100\% \quad (1)$$

In this equation, ΔH_f is the enthalpy of fusion of the samples and ΔH_f^0 (207 J/g) is the enthalpy of fusion of the 100% crystalline polypropylene [44]. The weight percent of MWCNT, w, was introduced in this equation to correct for the effect of nanoparticle content. The compression and microinjection molded samples were also examined by wide angle X-ray diffraction (WAXD). The tests were carried out using a Bruker AXS X-Ray goniometer equipped with a Hi-STAR two-dimensional area detector. The generator voltage and current were 40 kV and 40 mA, respectively and the copper Cu Kα radiation ($\lambda = 1.542$ Å) was selected by a graphite crystal monochromator.

Electrical Conductivity Measurements

The volume resistivity of the nanocomposites were determined by measuring the DC resistance across the thickness of compression molded disks using a Keithley electrometer model 6517 equipped with a two probe test fixture. All the connections were made using short wires to insure that the resistivity of the whole set up was negligible. The resistivity of the set up was measured each time before the tests to make sure that the system was working properly. This equipment allows resistance measurements up to 10^{17} Ω. The applied voltage, adapted to the expected resistance, was in the range of 1000 V for the neat polymers and samples containing up to 1wt% MWCNT and 100 V for samples containing 2 wt% and more MWCNTs. However, since for the more conductive samples, the accuracy of this equipment failed, samples containing more than 1 wt% MWCNTs were tested using the more adequate Keithley electrometer model 6220 connected to a current source (Aligent 34401 A, 6 [1/2] Digit Multimeter). For each sample the *I-V* curve was obtained and the sample resistance was determined from the slope of the curve. The resistance was then converted to volume resistivity, ρ_v, using the formula

$$\rho_v = AR_v/D \quad (2)$$

where A is the contact surface area, D is the thickness of the sample, and R_v is the measured resistance. The electrical conductivity (σ) of the nanocomposites is the inverse of volume resistivity. Prior to measurements all samples were dried under the conditions previously described.

Mechanical Properties

An Instron Micro Tester model 5548 was used to measure the tensile strength, modulus and elongation at break of the nanocomposites using microinjected tensile bars having a gage length of 4.3 mm. The tests were performed at room temperature using a crosshead speed of 50 mm/min, based on ASTM D638, and acquisition rate of 13 data per second. The tensile strength and elongation at break could be directly obtained from the stress-strain curves. To obtain the elastic modulus, a linear regression technique was utilized to define the slope of the stress-strain curve in the initial region before yield. All the reported values were averaged over six specimens for each composition with a maximum deviation of ±8%.

RESULTS

Morphology

SEM micrographs of the surfaces of compression molded and microinjected samples for the nanocomposites of 3wt% MWCNTs in PP and 5wt% MWCNTs in PC are shown in Fig. 2. It is worth mentioning that when the surface of the PP sample is chemically etched the presence of nanotubes can be better detected. It is clear that for the polypropylene nanocomposites, nanotube aggregates are formed and the distribution is not uniform (Fig. 2a). In contrast the nanotubes are well dispersed in the polycarbonate matrix and the distribution at the micro level is quite uniform (Fig. 2b). The presence of nanotube aggregates even after improving the mixing conditions and using PP-g-MA as a compatibilizer indicates that polypropylene is a difficult host, in the sense that the carbon nanotubes were not fully dispersed as individual entities. Although some small aggregates were also seen in the PC/MWCNT nanocomposites most of the nanotubes were dispersed individually even under the most unfavorable conditions.

These results reveal clearly a large difference between the compatibility of MWCNTs with PC as a polar amorphous polymer and with PP as a nonpolar polymer with a high degree of crystallinity. Because of the presence of strong polar-polar bonds, the nanotubes are better dispersed in PC without the formation of many aggregates; for polypropylene the lack of such polar bonds results in a poor dispersion of the nanotubes. In addition, the growth of the crystalline phase in the later case may result in the expulsion of the nanotubes towards the amorphous phase and lead to the formation of large aggregates in the PP-based nanocomposites [20].

Figure 2 also indicates that the nanotubes are somehow better distributed in the case of the microinjected samples. The drastically high deformation rates in microinjection molding contribute strongly to the nanotube distribution within the polymer matrix. In the case of the PP/MWCNT nanocomposites, the formation of smaller crystals in the

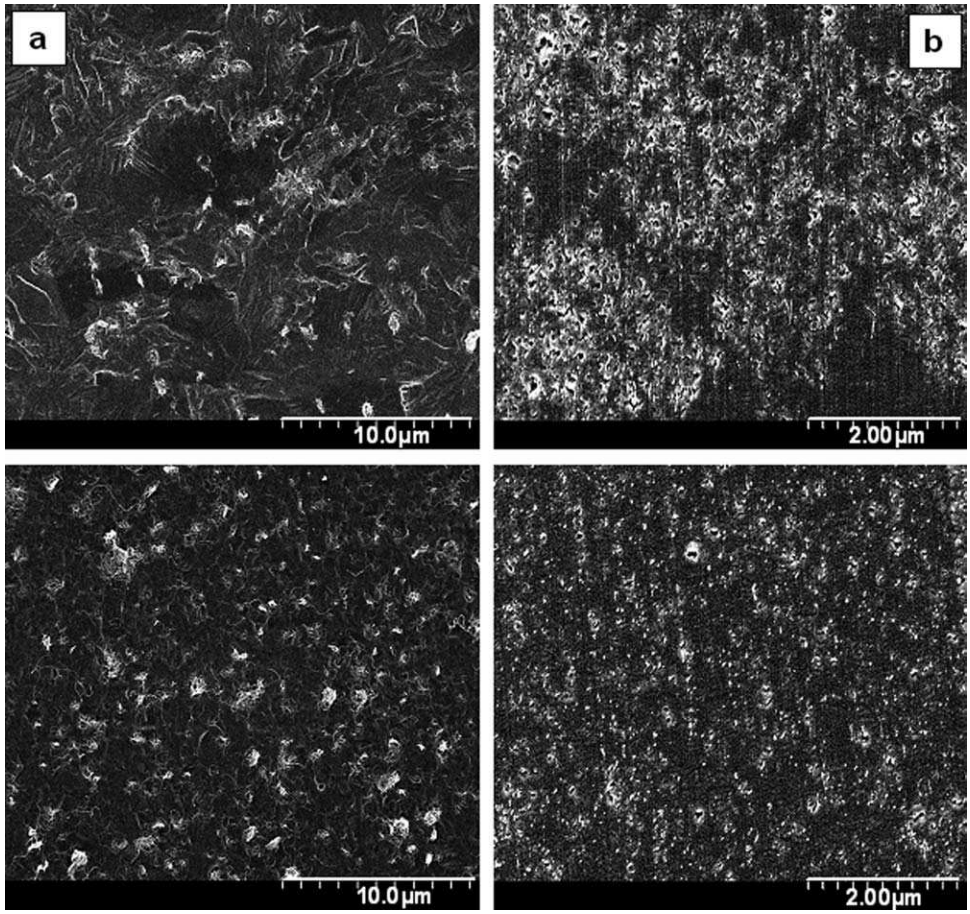

FIG. 2. SEM micrographs of (a) etched surface of PP/3wt% MWCNT and (b) crayon surfaces of PC/5wt% MWCNT nanocomposites. The top and the bottom micrographs are related to the compression molded and microinjected samples, respectively.

microinjected samples with the same degree of crystallinity (as it will be shown later) may be considered as another cause for the better distribution of the nanotubes. In fact, at constant degree of crystallinity, smaller crystals create narrower and more distributed path for amorphous phase located between them. However, aggregates are still observed in these samples. On the other hand, since the nanocomposite electrical conductivity is one of the main interest of this work, a well dispersed system may not be required for the formation of an electrically conductive network. As Fig. 3 shows for both PP and PC nanocomposites, an interconnected network of entangled MWCNTs exists forming a percolated network. This network seems to be even stronger and more efficient in the case of the PP nanocomposites in spite of worse dispersion quality. The presence of a crystalline phase in the PP matrix creates a structure similar to the case of a two-phase polymer blend with one phase being the crystals and the other phase the amorphous domain [45]. From a thermodynamic point of view, fillers and other kinds of impurities can never exist in a crystal [41, 46, 47] and, therefore, nanotubes are expected to be found only in the amorphous phase. The white and somehow parallel strips seen in Fig. 3a, indicated by the arrows, are the lamellae edge of crystals. The crystalline phase rejects the nanotubes to the edges of the lamellae during the crystallization growth stage. Therefore, as the figure illustrates, the nanotubes are located in the amorphous phase between the lamellae and form a continuous path in this blend-like structure. Consequently according to the concept of double percolation threshold a strong nanotube network is formed even at lower content compared to what is observed in the PC/MWCNT nanocomposites. The overall percolation threshold in PP is equal to the threshold of the amorphous phase, which is a fraction of the polymeric matrix, and therefore fewer nanotubes are needed to create a conductive network.

The formation of networks and the quality of the dispersion can be observed more clearly in TEM micrographs (see Fig. 4). The micrographs show some isolated nanotubes (particularly in the PP case) although most of them are grouped in dispersed bundles. In spite of the nonuniform dispersion in the PP nanocomposites (Fig. 4a), a strong connection between the nanotubes and consequently a complete network provide a suitable conductive pathway for the electrical current. In the PC

 DOI 10.1002/pen

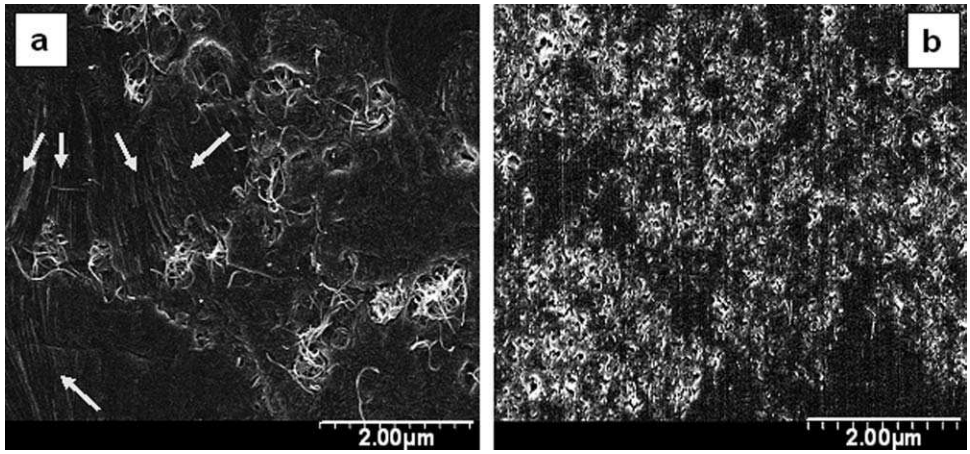

FIG. 3. High resolution SEM micrographs of (a) etched surface of PP/3wt% MWCNT and (b) crayon surfaces of PC/5wt% MWCNT nanocomposites. The arrays indicate the lamellae of the formed spherulites of PP.

nanocomposites (Fig. 4b), the nanotubes are well dispersed within the samples and the nanotube network seems to be not as well connected as that formed in the PP nanocomposites.

Crystallization and Crystalline Structure

Carbon nanotubes are well known to impart profound changes to the crystallization behavior of semicrystalline polymers [48, 49]. The presence of nanotubes provides a tremendous amount of heterogeneous nucleation sites for crystallization as they act as effective nucleating agents [48, 50]. The overall crystallization process is therefore expected to be accelerated as a result of this heterogeneous nucleation process. The effects of nanotube loading on the crystallization and crystalline characteristics of PP/MWCNT nanocomposites were examined using DSC. Figure 5 shows the DSC thermograms recorded during the first heating and cooling cycles for microinjection molding samples of various nanotube loadings. The thermograms recorded from the first heating of the compression molded samples (not shown here) were also analyzed and the results were compared as follows. The peak crystallization temperature is reported in Table 1 as T_C along with the melting temperature T_m and the degree of crystallinity for compression and microinjection molded samples. A slight difference in the melting behavior between the two types of samples can be seen: a higher melting point is recorded for microinjected samples with up to 1% nanotube content, suggesting the presence of more perfected crystals possibly due to higher molecular orientation. This distinction in the melting behavior is totally absent in the 5% nanotube sample. When analyzing the cooling portion of the thermograms no such a distinction between the compression and microinjection molded samples could be made for all nanotube concentrations. However, it is obvious that the crystallization onset temperature and the peak temperature increase with nanotube concentration. This suggests that crystal nucleation takes largely place at the surface of

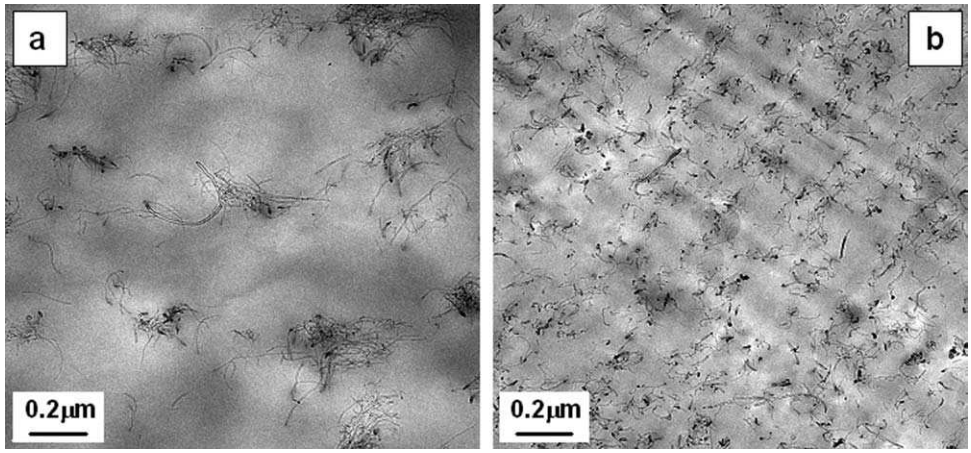

FIG. 4. TEM micrographs of thin sections of (a) PP/3wt% MWCNT and (b) PC/5wt% MWCNT nanocomposites.

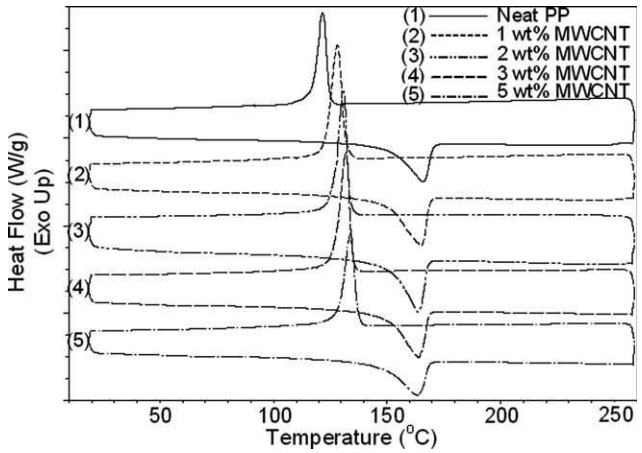

FIG. 5. First heating/cooling DSC thermograms - PP nanocomposites of various nanotube loadings - Arrows indicate thermograms for compression molded (black) and microinjection molded (blue) samples.

the MWCNTs. Furthermore, the results show that this effect is more pronounced at a lower MWCNT content than at higher content. As more nanotubes are added saturation of the nucleating sites is reached and the accelerating effect on the crystallization process disappears.

The overall crystallization rate due to the combined effects of nucleation and growth is affected by the crystallization temperature. The degree of supercooling or the difference between T_m and T_c is then a good indication of the crystallizability or crystallization rate. The smaller this difference, the larger the overall rate [51]. As Fig. 5 and Table 1 show T_c increases significantly with nanotube loading, while the effect is not so pronounced in the case of T_m (particularly for the compression molded samples) and as a result the difference between T_m and T_c decreases with nanotube loading. From a thermodynamic point of view, a higher temperature decreases the melt viscosity and favors the mobility of the polymer chains towards the crystallizing surface and thus accelerates the growth process.

The half crystallization time ($t_{1/2}$), defined as the time required to reach 50% relative crystallinity, is usually reported to compare the rate of crystallization of different samples. The relative crystallinity is calculated by using the following equation [52]:

$$X_r = \int_{T_0}^{T} QdT \Big/ \int_{T_0}^{T_\infty} QdT \tag{3}$$

where Q is the heat flow at temperature T and T_0 and T_∞ are the onset and termination crystallization temperature, respectively. The time related to the current temperature can be calculated as follows:

$$t = (T_0 - T)/\mathrm{CR} \tag{4}$$

where CR is the cooling rate (10°C/min). The crystallization curves during cooling are reported in Fig. 6 as a function of time. As it is observed, the rate of crystallization increases with nanotube content and this effect is clearly more important at low nanotube loading.

The values for the degree of crystallinity of the nanocomposites of different nanotube content for compression, microinjected and microinjection-compression molded samples are reported in Table 1. In all cases, the results show first an increase then a decrease in the degree of crystallinity as a function of nanotube content. A MWCNT content below 2 wt% causes an increase in crystallinity. A decrease in crystallinity is observed for MWCNT contents larger than 2%. It will be shown thereafter basedon electrical conductivity that 2 wt% MWCNT is the critical amount of nanotubes for a network formation and electrical percolation threshold in PP nanocomposites. Polymer crystallization is controlled first by crystal nucleation and second by crystal growth. In this particular case, the addition of up to 2 wt% nanotubes to the PP matrix results in a rapid increase of the number of nucleating sites, an increase in the nucleation rate and the degree of crystallinity as well; above 2 wt% the rate of nucleation keeps increasing, albeit more slowly before leveling off. On the other hand, the formation of a nanotube network restricts the polymer chains motion and, therefore, the formed crystals cannot grow properly and, consequently, the overall crystallization decreases.

TABLE 1. Nonisothermal crystallization and melting parameter for various nanotube loadings for PP samples prepared in compression (C), microinjection-compression (M-C), and microinjection (M) molding.

		Crystallinity (%) (DSC results)			Crystallinity (%) (XRD results)	T_m (°C)	
MWCNT (wt%)	T_C (°C)	C	M-C	M	C	C	M
0	122.0	38.6	47.8	44.4	39.9	162.1	166.0
0.5	124.4	43.7	50.9	47.6	49.7	162.3	165.9
1	128.4	52.2	57.6	54.6	51.3	163.5	165.2
2	131.0	53.7	59.6	56.2	52.2	163.6	163.9
3	132.1	52.8	57.3	53.8	50.0	163.7	163.8
5	134.1	43.2	45.8	44.7	47.5	163.7	163.7

The degree of crystallinity of compression molded samples obtained from XRD results is also reported.

 DOI 10.1002/pen

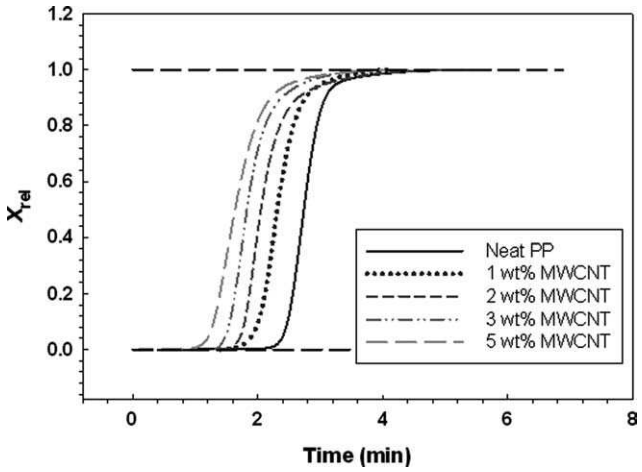

FIG. 6. Relative crystallinity as a function of time for different carbon nanotube loadings during the cooling cycle.

The effects of microinjection and microinjection-compression processing are shown in Table 1. Clearly these processes do not dramatically influence the crystallinity of the nanocomposites. The extremely high shear rates of these processes during the injection phase are expected to orient the polymer chains in the flow direction and to result in larger crystallinity. However, since injection is very fast and the whole cycle takes only few seconds, the chains do not have enough time to fully crystallize under the very high cooling rate. In microinjection-compression molding this effect is less pronounced as the cycle time is longer due to the compression phase and the cooling rate is slower. These, combined with applying a certain level of pressure after injection, result in a relatively larger crystallinity. The values of T_m for compression and microinjection samples are also shown in this table. It is well known that polymer chains are oriented under shear, and this results in a reduction of the entropy, S, of polymer melts. The equilibrium melting temperature is defined by [53]:

$$\Delta G = \Delta H - T_m^0 \Delta S = 0 \quad (5)$$

where ΔG is the free energy, ΔH and ΔS are the enthalpy and entropy of fusion, respectively. Considering that the enthalpy is not affected by flow, the equilibrium melting temperature must increase as a result of the entropy reduction [54]. For microinjection molded samples, in spite of short cycling time, the equilibrium melt temperature of the neat PP increases due to high deformation rate of the process, which results in highly oriented polymer chains. However, as shown in Table 1 there is no difference between the melting points for the 5 wt% nanocomposite samples obtained by compression and microinjection. Obviously, the presence of nanotubes hinders the polymer chain orientation. Accordingly, the influence of microinjection and microinjection-compression on the degree of crystallinity decreases with nanotube loading.

The effect of processing on crystallization and orientation of the crystalline phase was also considered using WAXD. The X-ray diffraction patterns obtained for the 5% PP/MWCNT composite are shown in Fig. 7. For the compression molded sample (Fig. 7a) whole rings are observed indicating random orientation. On the other hand, the diffraction patterns obtained from the microinjection sample (Fig. 7b) exhibit distinct and bright asymmetric arcs, a clear indication of a relatively high level of orientation. The corresponding 2θ diffraction intensity curves are shown in Fig. 7c. Both compression molded and microinjected samples show the same profile of the α-crystals of iPP and there is no effect of processing on the reflections indicating that the crystalline structure of iPP is not affected. After deconvolution of the peaks and from the area under the curves, the crystallinity was calculated and, similarly to DSC results, it was found that the degree of crystallinity increases up to 2 wt% nanotube loading and then decreases for larger loading. It can be noted, however, that the crystallinity obtained from WAXD is slightly different from that obtained using DSC (Table 1).

Electrical Conductivity

One of the stated objectives of this work was to investigate the effect of processing on the electrical conductivity of nanocomposites based on carbon nanotubes. Microinjection molding was chosen because it imparts a high

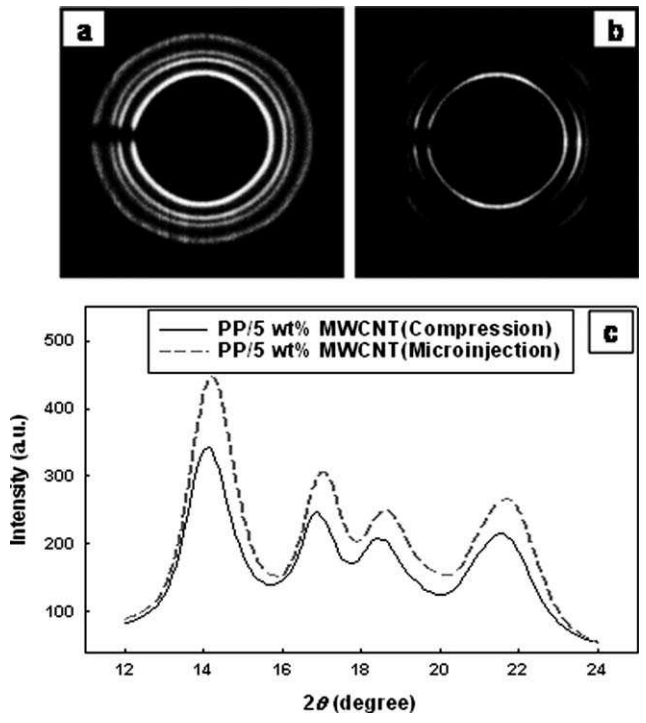

FIG. 7. WAXD pattern of 5 wt% PP/MWCNT nanocomposites for (a) compression molded, (b) microinjected samples. (c) Diffraction spectrum with integration through the circles.

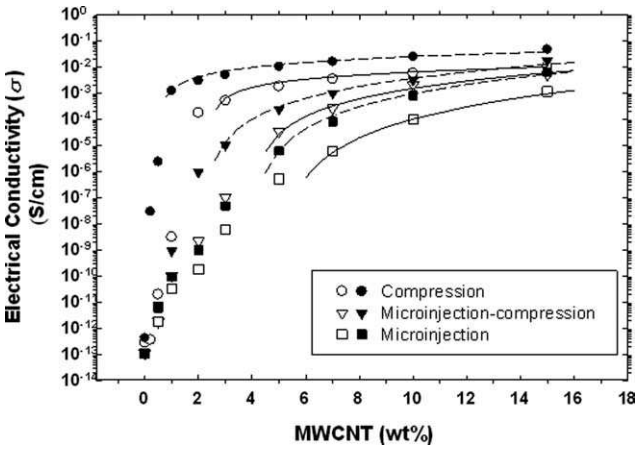

FIG. 8. Effect of polymer processing conditions on electrical conductivity and percolation threshold of the PP/MWCNT (filled symbols) and PC/MWCNT (open symbols) nanocomposites. The lines shown are the best fits of *Eq. 5*.

degree of shearing and orientation on the polymer chains and nanotubes as opposed to compression molding processing. Moreover, investigating electrical conductivity may be useful to the understanding of the relationship between the nanocomposite microstructure and the final properties of the microparts. Figure 8 presents the effect of the nanotube loading on the electrical conductivity of the disk shaped nanocomposite samples prepared by the same processing methods as previously.

The electrical conductivity above the threshold can be described by a power-law expression [6, 36]:

$$\sigma = \beta_{c,\sigma}\left(\frac{m - m_{c,\sigma}}{m_{c,\sigma}}\right)^{q} \text{ for } m \geq m_{c,\sigma} \tag{6}$$

where $\beta_{c,\sigma}$ and q are power-law constants and $m_{c,\sigma}$ is the electrical percolation threshold (wt%). This power-law expression is found to describe very well the data of Fig. 8 above the percolation threshold given by the left limit of the dashed line corresponds to the percolation threshold value in each case. For compression molded samples the percolation threshold is found to be around 3 wt% of nanotubes for the PC nanocomposites and around 1 wt% for the PP nanocomposites. At these critical concentration levels, the electrical conductivity rises suddenly by more than 10 decades and nanocomposites containing more than 1 and 3 wt% (in PP and PC, respectively) can be considered as electrically conductive. This sudden rise in the electrical conductivity is due to the formation of a network of connected nanotubes paths. Beyond this percolation threshold the electrical conductivity increases more gradually and asymptotically towards a plateau. This is a typical percolation behavior, which is usually observed in nanocomposites of conductive fillers and can be referred as an ideal percolation behavior [13, 55].

Conversely, as can be seen from Fig. 8, no step-like increase in electrical conductivity is observed for both PP- and PC-based nanocomposites prepared by microinjection. In the microinjected samples the nanotubes are well aligned in the flow direction due to the very high deformation rates of the process [36] and are less likely to interconnect. A conductive pathway resulting from a proximity effect would form only at high nanotube contents and consequently the percolation threshold is expected to rise. The percolation threshold of microinjected samples, as determined using *Eq. 6*, occurs at about 6 and 4 wt% of nanotubes loading in the PC and PP nanocomposites, respectively. Our preliminary results (not presented here) revealed that for a dog-bone shaped mold cavity, where the main flow is longitudinal, the percolation threshold is higher (about 9 wt%) and the electrical conductivities are about one order of magnitude lower than those of the disk shaped cavity samples. The radial flow of the centrally gated disk-shape cavity is largely elongational in the center zone while shear flow is dominant near the cavity walls [56]. This yields a more complex orientation of the nanotubes: in the radial direction near the walls and in the transverse or azimutal directions within the core. This mixed orientation leads to a more random overall orientation and more interaction between the nanotubes resulting in a lower electrical percolation threshold.

The electrical threshold pertaining to microinjection-compression molded samples is found to be close to the one obtained in compression molded samples. As described before, this process has two phases: an injection phase with a high deformation rate-low pressure step and a compression phase with low deformation rate-high pressure step. Because of the high deformation rate the nanotubes are well aligned near the cavity walls at the end of the first step or injection phase. However, the compression phase is similar to a squeeze flow, which forces the nanotubes to partially rearrange in the transverse direction and results in a somehow isotropic arrangement of the nanotubes. This is more favorable for the creation of a nanotube network. The effect of the presence of a crystalline structure on the electrical conductivity is also observed in Fig. 8. Clearly for all processes, the electrical conductivity is about one order of magnitude larger and the percolation threshold is somehow lower in the case of PP nanocomposite. This is explained by the concept of double percolation threshold. Polypropylene can be considered as a two-phase blend where the nanotubes are mostly located in the amorphous phase (as shown before in the morphological study). Accordingly there are two types of percolation in the nanocomposite at the same time: percolation resulting in the continuity of the filler-rich phase or amorphous phase and percolation of nanotubes in this phase.

Mechanical Property

Typical stress-strain curves of both PP/MWCNT and PC/MWCNT nanocomposites with respect to nanotube content are shown in Fig. 9. The neat PP presents the

 DOI 10.1002/pen

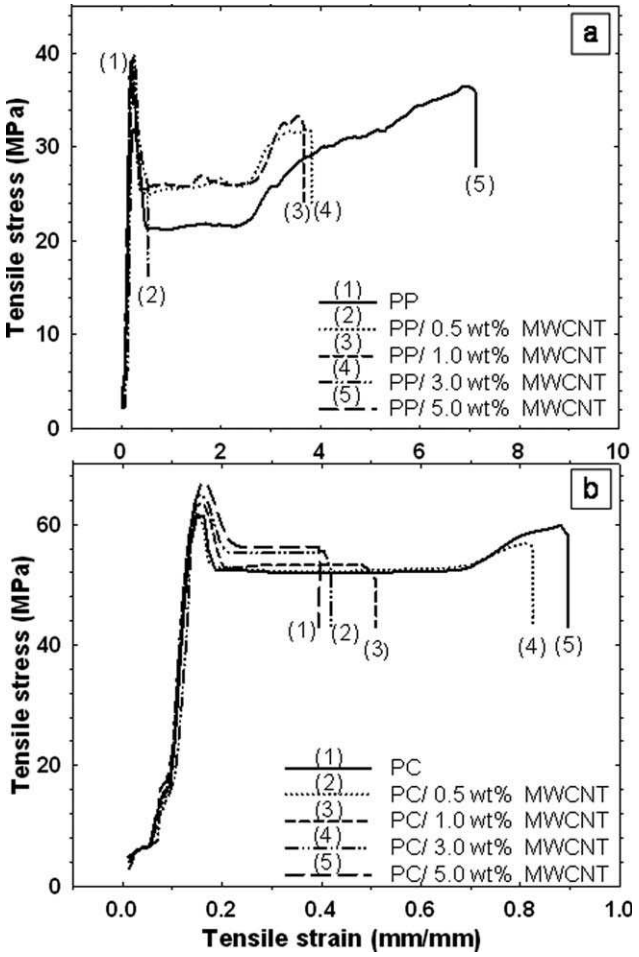

FIG. 9. Tensile behavior: stress-strain diagrams of (a) PP/MWCNT and (b) PC/MWCNT composites.

typical behavior of a ductile material with a very large elongation value at break (700%). At about 250% of elongation strain hardening begins and then the tensile stress increases almost linearly with strain until fracture or break eventually occurs. In the case of nanocomposites with

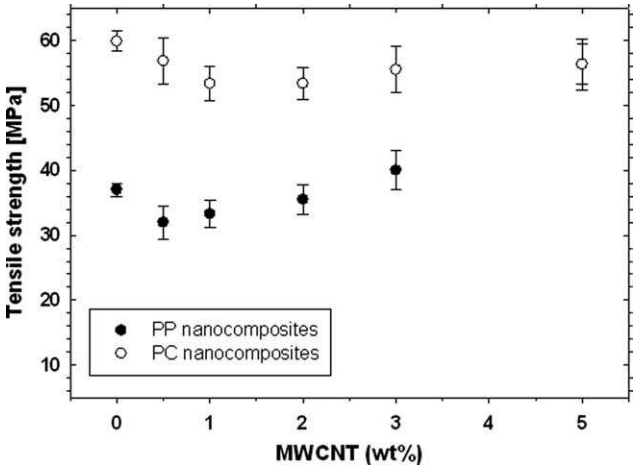

FIG. 10. Tensile strength of dog-bone shaped microinjected PP/MWCNT and PC/MWCNT samples.

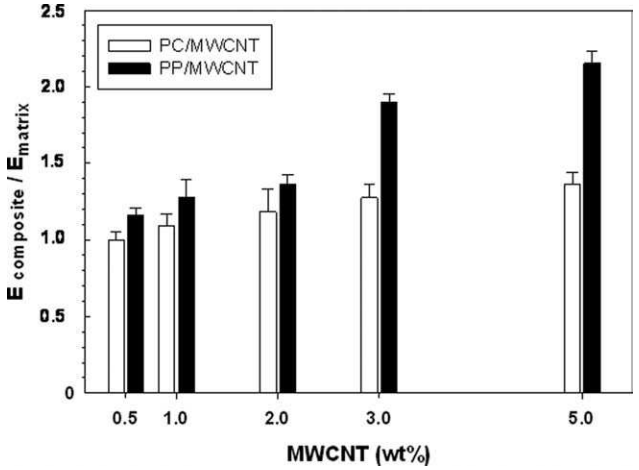

FIG. 11. Relative Young modulus of PP/MWCNT and PC/MWCNT with respect to the neat polymers.

lower loading (0.5 and 1 wt% MWCNTs) the same ductile behavior is observed with necking and strain hardening but with significantly lower elongation at break. For the nanocomposites with higher nanotube contents (3 and 5 wt%), a brittle behavior is observed with breaking after the yield point. The neat PC shows the same ductile behavior with about eight times larger elongation value at break (90%). For the neat PC and the 0.5 wt% PC/nanocomposite strain hardening and necking at high elongation are observed. However, the nanocomposites with higher nanotube loadings show no strain hardening and become more brittle as the strain-to-failure decreases with nanotube concentration. All samples show yielding before exhibiting plastic flow.

As Fig. 9 reveals, the elongation values at break for the PP/MWCNT nanocomposites are about eight times larger than those of PC/MWCNT nanocomposites. However, in both cases, the values are strongly affected by nanotube loading, starting to decrease drastically beyond 1wt% of nanotube loading. The structural change of the nanocomposites with increasing nanotube content is probably responsible for this phenomenon. At a critical concentration, the formation of nanotubes aggregates or agglomerates induces a change in the load transfer behavior of the nanocomposites and results in a different trend in the mechanical properties.

The strength at break of the various nanocomposites is presented in Fig. 10 as a function of nanotube loading. As expected, the neat PC and its nanocomposites have larger strength values than the PP and its nanocomposites. However, in both cases the effect of nanotube loading on the nanocomposite strength is not very significant and the overall tendency demonstrates only a modest increase with MWCNT concentration. This could probably be due to the poor interaction between the nanotubes and polymer chains so that the nanotubes could not demonstrate their theoretical potential as a very strong filler with extremely high strength [57]. We also observe first a

slight decrease of the strength at break then an increase with MWCNT loading after 1 wt% in PC and after 2 wt% in PP, probably due to the formation of nanotube networks at these concentrations.

The effect of MWCNT loading on the Young modulus of the nanocomposites is shown in Fig. 11. In order to compare the effect of nanotubes on the modulus of PP and PC, the raw values are normalized with respect to the neat polymer modulus. It is observed that the addition of nanotubes significantly affects the Young modulus of PP while the effect is less significant in the case of the PC/MWCNT nanocomposites. The modulus of the PP increases by more than 90% with only 3 wt% of nanotubes largely due to the increased degree of crystallinity, while for the PC the increase is considerably less, about 30% for the same nanotube content. However, the rate of increase of the elastic modulus is quite modest for larger nanotube loadings.

CONCLUSIONS

In this work we have examined the effects of crystalline structure and polymer processing on PP/MWCNT and PC/MWCNT nanocomposite properties. Three different polymer processing methods, compression molding, microinjection-compression molding and microinjection molding have been investigated. The study of the crystalline behavior of PP/MWCNT nanocomposites revealed that the presence of the nanotubes significantly affected the nanocomposite structure. The degree of crystallinity went through a maximum at 2 wt % nanotube and then the crystallinity decreased due to the formation of nanotube networks, which restricted the polymer chains motion and slowed down the crystal growth. It was also found that the high deformation values of the microinjection molding only slightly changed the overall crystallinity because of very short cycle time of the process. However, the crystals were all oriented in the flow direction.

Interestingly, changing the type of processing strongly affected the electrical conductivity of the nanocomposites. The percolation thresholds rose significantly in both PP and PC nanocomposites using processing involving larger deformation rates. In these cases no neat percolation threshold was observed. The presence of a crystalline structure was also found to improve the electrical conductivity of PP/nanocomposites according to the concept of double percolation threshold. The strength and modulus of the nanocomposites were also found to be significantly improved by the addition of nanotubes especially in case of the PP/MWCNT nanocomposites. However, the elongation at break was found to decrease significantly with nanotube content.

ACKNOWLEDGMENTS

The authors are also thankful to Ms. Weawkamol Leelapornpisit for her great help in the morphological studies. Financial support from NSERC (Natural Science and Engineering Research Council of Canada) is gratefully acknowledged.

REFERENCES

1. S. Iijima, *Nature*, **354**, 6348 (1991).
2. S. Iijima and T. Ichihashi, *Nature*, **363**, 6430 (1993).
3. M. Meyyappan, *Carbon Nanotubes: Science and Applications*, CRC Press, Boca Raton (2005).
4. O. Meincke, D. Kaempfer, H. Weickmann, C. Friedrich, M. Vathauer, and H.O. Warth, *Polymer*, **45**, 739 (2004).
5. M. Moniruzzaman and K.I. Winey, *Macromolecules*, **39**, 5194 (2006).
6. G. Hu, C. Zhao, S. Zhang, M. Yang, and Z.G. Wang, *Polymer*, **47**, 480 (2006).
7. Y.T. Sung, M.S. Han, K. H. Song, J.W. Jung, H.S. Lee, C.K. Kum, J. Joo, and W.N. Kim, *Polymer*, **47**, 4434 (2006).
8. G.T. Pham, Y.B. Park, S. Wang, Z. Liang, B. Wang, C. Zhang, P. Funchess, and L. Kramer, *Nanotechnology*, **19**, 325705 (2008).
9. W.Y. Wang, G.H. Luo, F. Wei, and J. Luo, *Polym. Eng. Sci.*, **49**, 2144 (2009).
10. L. Karasek and M. Sumita, *J. Mater. Sci.*, **31**, 281 (1996).
11. M. Sumita, S. Asai, N. Miyadera, E. Jojima, and K. Miyasaka, *Colloid Polym. Sci.*, **264**, 212 (1986).
12. M. Sumita, H. Abe, H. Kayaki, and K. Miyasaka, *J. Macromol. Sci., Part B*, **25**, 171 (1986).
13. D. Wu, L. Wu, W. Zhou, T. Yang, and M. Zhang, *Polym. Eng. Sci.*, **49**, 1727 (2009).
14. P. Potschke, A.R. Bhattacharyya, and A. Janke, *Carbon*, **42**, 965 (2004).
15. J. Zeng, B. Saltysiak, W.S. Johnson, D.A. Schiraldi, and S. Kuma, *Compos. B*, **35**, 173 (2004).
16. B. Lin, U. Sundararaj, and P. Pötschke, *Macromol. Mater. Eng.*, **291**, 227 (2006).
17. F. Du, R.C. Scogna, W. Zhou, S. Brand, J.E. Fischer, and K.I. Winey, *Macromolecules*, **37**, 9048 (2004).
18. J.K.W. Sandler, J.E. Kirk, I.A. Kinloch, M.S.P. Shaffer, and A.H. Windle, *Polymer*, **44**, 5893 (2003).
19. K. Jeon, L. Lumata, T. Tokumoto, E. Steven, J. Brooks, and R.G. Alamo, *Polymer*, **48**, 4751 (2007).
20. S.C. Tjong, G.D. Liang, and S.P. Bao, *Polym. Eng. Sci.*, **48**, 177 (2008).
21. M. Sumita, K. Sakata, S. Asai, K. Miyasaka, and H. Nakagawa, *Polym. Bull.*, **25**, 265 (1991).
22. M. Sumita, K. Sakata, Y. Hayakawa, S. Asai, K. Miyasaka, and M. Tanemura, *Colloid Polym. Sci.*, **270**, 134 (1992).
23. V. Tan and M.R. Kamal, *J. Appl. Polym. Sci.*, **22**, 2341 (1978).
24. C. Kukla, H. Loibl, and H. Detter, *Kunstsoffe Plast, Europe* **88**, 6 (1998).
25. B. Sha, S. Dimov, C. Griffiths, M.S. Packianather, *Int. J. Adv. Manuf. Technol.*, **33**, 147 (2007).
26. J. Zhao, R.H. Mayes, G. Chen, H. Xie, and P.S. Chan, *Polym. Eng. Sci.*, **43**, 1542 (2003).

27. C.H. Wu and W.J. Liang, *Polym. Eng. Sci.*, **45**, 1021 (2005).
28. Y.C. Su, J. Shah, L. Lin, *J. Micromech. Microeng.*, **14**, 415 (2004).
29. R.D. Chien, *Sens. Actuators, A: Phys.*, **128**, 238 (2006).
30. C.K. Huang, *Eur. Polym. J.*, **42**, 2174 (2006).
31. C.K. Huang, S.W. Chen, and C.T. Yang, *Polym. Eng. Sci.*, **45**, 1471 (2005).
32. S. Abbasi, P.J. Carreau, and A. Derdouri, *Polymer*, **51**, 922 (2010).
33. W. Ding, A. Eitan, F.T. Fisher, X. Chen, D.A. Dikin, R. Andrews, L.C. Brinson, L.S. Schadler, and R.S. Ruoff, *Nano Lett.*, **3**, 1593 (2003).
34. S. Singh, Y. Pei, R. Miller, and P.R. Sundararajan, *Adv. Funct. Mater.*, **13**, 868 (2003).
35. P. Potschke, M. Abdel-Goad, I. Alig, S. Dudkin, and D. Lellinger, *Polymer*, **45**, 8863 (2004).
36. S. Abbasi, P.J. Carreau, A. Derdouri, and M. Moan, *Rheologica Acta*, **48**, 943 (2009).
37. X. Chen, J. Hu, L. Zhou, W. Li, Z. Yang, Y. Wang, *J. Mater. Sci. Technol.*, **24**, 279 (2008).
38. T.E. Chang, L.R. Jensen, A. Kisliuk, R.B. Pipes, R. Pyrz, and A.P. Sokolov, *Polymer*, **46**, 439 (2005).
39. A.A. Koval'chuk, A.N. Shchegolikhin, V.G. Shevchenko, P.M. Nedorezova, A.N. Klyamkina, and A.M. Aladyshev, *Macromolecules*, **41**, 3149 (2008).
40. K. Prashantha, J. Soulestin, M.F. Lacrampe, P. Krawczak, G. Dupin, and M. Claes, *Compos. Sci. Technol.*, **69**, 1756 (2009).
41. H.G. Kilian, G. Lagaly, and I. Chudacek, "Relationships of Polymeric Structure and Properties," *Progress in Colloid and Polymer Science*, *Vol. 78*, Springer, Berlin/Heidelberg (1988).
42. P. Potschke, T.D. Fornes, and D.R. Paul, *Polymer*, **43**, 3247 (2002).
43. D.W. Litchfield and D.G. Baird, *Polymer*, **49**, 5027 (2008).
44. G.W. Lee, S. Jagannathan, H.G. Chae, M.L. Minus, and S. Kumar, *Polymer*, **49**, 1831 (2008).
45. L.E. Nielsen and R.F. Landel, *Mechanical Properties of Polymers and Composites*, 2nd ed., Marcel Dekker, New York (1993).
46. A. Sharples, *Introduction to Polymer Crystallization*, St. Martin's Press, New York (1966).
47. T.S. Nordmark and G.R. Ziegler, *Carbohydrate Polym.*, **49**, 439 (2002).
48. D. Wu, L. Wu, G. Yu, B. Xu, and M. Zhang, *Polym. Eng. Sci.*, **48**, 1057 (2008).
49. J.Y. Kim., S.-I. Han, S.H. Kim, *Polym. Eng. Sci.*, **47**, 1715 (2007).
50. S.Y. Lin, E.C. Chen, K.Y. Liu, and T.M. Wu, *Polym. Eng. Sci.*, **49**, 2447 (2009).
51. C.-F. Ou, M.-S. Chao, S.-L. Europ, *Polym. J.*, **36**, 2665 (2000).
52. V.A. Alvarez, P.M. Stefani, and A. Vázquez, *J. Thermal Anal. Calorimetry*, **79**, 187 (2005).
53. B. Monasse, *J. Mater. Sci.*, **30**, 5002 (1995).
54. T.W. Haas and B. Maxwell, *Polym. Eng. Sci.*, **9**, 225 (1969).
55. X. Feng, G. Liao, J. Du, L. Dong, K. Jin, and X. Jian, *Polym. Eng. Sci.*, **48**, 1007 (2008).
56. M. Vincent, E. Devilers, and J.F. Agassant, *J. Non-Newton Fluid Mech.*, **73**, 317 (1997).
57. Z. Fang, J. Wang, and A. Gu, *Poly. Eng. Sci.*, **46**, 670 (2006).